What is the meaning of hydrogen-to-carbon ratio determined in Archean organic matter?

Frédéric Delarue, Sylvie Derenne, Kenichiro Sugitani, François Baudin, Frances Westall, Barbara Kremer, Romain Tartese, Adriana Gonzalez, François Robert

What is the meaning of Hydrogen-to-Carbon ratio determined in Archean organic matter?

Frédéric Delarue[1*], Sylvie Derenne[2], Kenichiro Sugitani[3], François Baudin[4], Frances Westall[5], Barbara Kremer[6], Romain Tartèse[7], Adriana Gonzalez[1], François Robert[1]

[1]*Muséum National d'Histoire Naturelle, Sorbonne Université, UMR CNRS 7590, IRD, Institut de Minéralogie, de Physique des Matériaux et de Cosmochimie, IMPMC, 75005 Paris, France.*

[2]*Sorbonne Universités, UPMC Univ Paris 06, CNRS, UMR 7619 METIS, 4 place Jussieu, F-75005 Paris, France.*

[3]*Department of Environmental Engineering and Architecture, Graduate School of Environmental Studies, Nagoya University, Nagoya, Japan.*

[4]*Sorbonne Université, UPMC Univ. Paris 06, CNRS, UMR 7193 ISTeP, 4 place Jussieu, F-75005 Paris France.*

[5]*Centre de Biophysique Moléculaire, UPR CNRS 4301, rue Charles Sadron, 45071 Orléans Cedex 02, France*

[6]*Institute of Paleobiology, Polish Academy of Sciences, Twarda 51/55, 00-818 Warszawa, Poland*

[7]*School of Earth and Environmental Sciences, University of Manchester, Manchester, M13 9PL, UK*

*corresponding author, fdelarue@mnhn.fr

Abstract

The search for hydrocarbon molecular biomarkers in Archean metasediments is of prime importance for deciphering the early evolution of life. Suitable criteria are required to identify promising targets for further molecular biomarkers. Possible criteria include the Hydrogen-to-Carbon (H/C) atomic ratio used as a proxy of the aliphatic content of the kerogen matrix. However, H/C ratio values exhibit large variation in Archean kerogens and their significance remains poorly understood. In this study, we thus investigate the significance of the H/C ratios of Archean kerogens by combining elemental analyses, Nanoscale Secondary Ion Mass Spectrometry (NanoSIMS), Rock-Eval pyrolysis and Raman spectroscopy. First, NanoSIMS investigations show the H/C ratio of kerogen can be compromised by residual minerals. In addition, Rock-Eval pyrolysis underlines the fact that thermal cracking of Archean kerogens does not just release hydrocarbon covalently linked to the macromolecular network but also a complex mixture of organic pools distinguished by their thermal maturity. Therefore, the H/C ratio alone cannot be used to probe the preservation of aliphatic compounds bound to kerogen since it can be biased by the presence of (i) residual bitumen, as well as (ii) refractory organic matter in secondary hydrothermal veins whose syngenecity is debatable. Rock-Eval pyrolysis then provides a useful and complementary method to check the significance of H/C atomic ratio as a proxy for hydrocarbon preservation in Archean kerogens.

Keywords: Bitumen, Carbonization, Early life, Kerogen, NanoSIMS, Precambrian, Raman, Rock-Eval pyrolysis

1. Introduction

The origin of the oldest traces of life on Earth has been investigated through chemical and thermal degradation of organic matter (OM) from Archean silicified sediments (Brocks et al., 1999, 2003a; Marshall et al., 2007; Ventura et al., 2007; Derenne et al., 2008). In addition to the numerous debates about the syngenecity of putative molecular biomarkers (Marshall et al., 2007; Rasmussen et al., 2008; French et al., 2015), the preservation of aliphatic moieties in OM from Archean silicified sediments remains an open issue (Bourbin et al., 2012a). Thus, French et al. (2015) highlighted the need to identify promising targets for further hydrocarbon biomarker investigation by combining various approaches such as elemental analyses, Raman spectroscopy and Rock-Eval pyrolysis.

In contrast to soluble hydrocarbons thought to be highly sensitive to contamination, hydrocarbons released through the thermal cracking of covalent bonds of the insoluble OM, the so-called kerogen macromolecular structure, are considered syngenetic (Brocks et al., 2003b; Marshall et al., 2007; Derenne et al., 2008). Because of thermal alteration extending to greenschist/amphibolite facies metamorphism in Archean metasediment (Westall et al., 2006; Sugitani et al., 2007; 2015; Delarue et al., 2016), the macromolecular network of Archean kerogens is often depleted in aliphatic moieties (Bourbin et al., 2012a) as

reflected by Hydrogen-to-Carbon (H/C) atomic ratios mostly below 0.3 (Hayes et al., 1983; Marshall et al., 2007). Nevertheless, several studies indicated that some Archean kerogens can also be characterized by H/C atomic ratios higher than 0.3, reaching values up to 0.6 (Hayes et al., 1983; Marshall et al., 2007; Derenne et al., 2008; French et al., 2015; Ferralis et al., 2016). A H/C atomic ratio up to 0.6 in kerogen from the 3.45 Gyr-old Warrawoona Formation (Derenne et al., 2008) has been considered inconsistent with the prehnite-pumpellyite and lower greenschist facies metamorphism undergone by the host rock (Marshall et al., 2007). This interpretation points toward the presence of aliphatics that do not belong to the Archean kerogen. Thus, additional H source(s) may have compromised the use of H/C atomic ratio as an indicator of aliphatic hydrocarbon covalently linked to the kerogen matrix. Moreover, the syngenecity of additional hydrocarbon sources can be questioned, because only hydrocarbons linked to the kerogen are definitely considered as syngenetic, as stressed above.

As a screening tool to depict OM quality, Rock-Eval pyrolysis provides quantitative information about the composition of OM through the Total Organic Carbon (TOC) content and the Hydrogen and Oxygen Indices (HI and OI), the latter two being correlated with H/C and O/C ratios, respectively (Espitalié et al., 1977; 1985a; 1985b; Peters, 1986). Beyond these parameters, Rock-Eval pyrolysis also provides information to characterize source/reservoir rocks and kerogens as part of petroleum exploration. Thus, S1 peaks (effluents released during an isothermal heating at 300°C) are widely recognized as being related to free and adsorbed compounds whereas S2 peaks (effluents released during pyrolysis above

300°C) are usually attributed to the thermal cracking of insoluble OM (Romero-Sarmiento et al., 2016). However, (i) solid bitumen, i.e. insoluble OM formed during the solidification of generated bitumen (Curiale, 1986; Jacob, 1989; Sanei et al., 2015), and (ii) heavy bitumen can yield significant amounts of hydrocarbons in the S2 peak, especially in the 350-450ºC range (Delvaux et al., 1990; Grundman et al., 2012; Jarvie, 2012; Han et al., 2015; Hackley and Cardott, 2016). Thus, an S2 peak may be produced by the thermal cracking of a composite organic mixture consisting of kerogen, solid bitumen and heavy bitumen which can bias HI determination but also the quantitative assessment of the thermal maturity of kerogen through the Rock-Eval-derived TpkS2 parameter, the temperature corresponding to the maximum release of hydrocarbons during pyrolysis of kerogen (Espitalié, 1986; Behar et al., 2001).

A large part of Archean metasediments underwent hydrothermalism leading to their induration through early silicification, which drastically reduced rock porosity (Ledevin et al., 2014). Silicification may have then limited OM migration during thermal alteration provided that silicification was nearly contemporaneous with sedimentary OM deposition on Archean seafloors. If correct, Archean silicified metasediments should act as a source-reservoir system possibly containing a mixture of kerogen, solid bitumen and heavy bitumen, which may in turn explain why some Archean OM have high H/C atomic ratios that seem at odds with their thermal alteration. However, such an issue remains undocumented although Rock-Eval pyrolysis has been used to characterize Archean OM, focusing on the determination of the TOC content, the HI index and the TpkS2 (Brocks et al., 2003b, Spangenberg and Frimmel, 2004; Marshall et

al., 2007; French et al., 2015). Thus, Brocks et al. (2003) reported that pyrolysis of ca. 2.7 Gyr-old kerogen did not yield enough hydrocarbons to provide reliable HI and TpkS2 values, in line with the low H/C ratio usually observed in Archean kerogens. To date, Rock-Eval pyrolysis has not been applied to Archean kerogens exhibiting unusually high H/C ratio (in comparison to most Archean kerogens), although a careful analysis of the pyrograms would help in determining whether the aliphatic hydrocarbons are covalently linked to the kerogen macromolecular network.

Our purpose was therefore to study the significance of the H/C atomic ratio determined on isolated Archean OM, exploring the occurrence of additional H sources. To this end, isolated Archean OM samples were investigated by Rock-Eval pyrolysis. In addition, Nanoscale Secondary Ion Mass Spectrometry (NanoSIMS) was performed on selected isolated Archean OM characterized by distinct H/C ratios to check whether H/C atomic ratios were biased by H in remaining minerals. Finally, the syngenecity of additional H sources was addressed using Raman spectroscopy.

2. Material and Methods

2.1. Studied sites

Organic matter was isolated from 12 Archean cherts (Table 1). Seven Farrel Quartzite samples (GGR2, GRW10, ORW9, GFWEX1-1b, MGTKS1up, MGTKS1 and MGTKS3 samples; 3.0 Ga; Table 1) were collected from the Goldsworthy

144 greenstone belt in the Pilbara Craton, Western Australia. Three samples
145 (GFWEX1-1b, MGTKS1 up and MGTKS1) are bedded black chert and contain
146 microfossils (Sugitani et al., 2007; Delarue et al., 2017; Tartèse et al., 2017). They
147 are assumed to have been deposited in a shallow evaporitic basin with input of
148 hydrothermal fluids (Sugahara et al., 2010). GGR2 is a black chert interbedded
149 with sandstone from the lower unit of the Farrel Quartzite. ORW9 and GRW10
150 are laminated black cherts from the cherty succession, which conformably
151 overlies the Farrel Quartzite that is assigned to the Cleaverville Formation.
152 The 99SA07 chert (3.3 Ga; Table 1) was sampled in the Barberton greenstone
153 belt, Onverwacht Group, located in the upper part of the Josefsdal Valley, South
154 Africa. The Josefsdal chert sample consists of silicified volcaniclastic sediments.
155 It is laminated and contains phyllosilicate grains and silica veins (Westall et al.,
156 2006).
157 The 07SA22 chert (3.4 Ga; Table 1) was sampled in the Barberton greenstone
158 belt, South Africa. It consists of silicified detrital sediment comprising volcanic
159 grain, fluid inclusions, and CM floccules (Bourbin et al., 2012b).
160 The 4 of 03/08/85 chert (3.4 Ga; Table 1) was collected in the Warrawoona Group,
161 Pilbara Craton, Marble Bar Greenstone Belt, Western Australia. It mainly
162 consists of revealed large micro-crystalline silica grains, fractures filled with
163 quartz and OM floccules (Bourbin, 2012).
164 The microfossil-bearing Panorama chert (3.4 Ga; Table 1) has been identified in
165 the East Pilbara Terrane of the Pilbara Craton, Western Australia. This
166 formation is typically of 8–11 m thickness and is composed of various rocks types,
167 including siliciclastic sedimentary rocks such as sandstone and shale, carbonates

(mainly bedded and stromatolitic dolomite), chert, and volcaniclastic rock (Sugitani et al., 2015).

In addition to Archean samples, OM from the Silurian "Zalesie Nowe"chert (Holy Cross Mountains, Bardo Syncline, Poland) was studied as a reference for immature kerogen (Table 1). Zalesie Nowe is representative of typical Paleozoic primary cherts composed of cryptocrystalline and mostly homogeneous quartz with a small admixture of phyllosilicate minerals. The Zalesie Nowe chert is distinctly laminated and consists of well-defined, horizontally extended undulating laminae that are 10–40 cm thick and composed of amorphous dark brown to brownish-red organic material. OM has been identified mostly as fossil remnants of algae and benthic cyanobacterial mats. Graptolites indicate a Llandovery (early Silurian) age for these samples (Kremer and Kazmierczak, 2005).

2.2. Organic Matter Isolation

Isolation of OM was performed on about *ca.* 300 g of crushed rock. Carbonates were removed at room temperature using hydrochloric acid (HCl; 37%; reagent grade) to minimize the formation of fluorides during hydrofluoric acid (HF)/HCl maceration. Samples were then centrifuged and washed with distilled water until reaching neutrality. Concentration of OM was achieved through acid maceration at room temperature in a mixture of HF (40%, reagent grade) and HCl (2/1, v/v; reagent grade). Samples were centrifuged and washed with distilled water to reach neutrality. Neoformed fluorides were then degraded using HCl (37%;

192 reagent grade) at 60°C (24 hours). After HCl hot acid maceration, the isolated
193 OM matter was centrifuged/washed with distilled water until reaching
194 neutrality. Finally, samples were air-dried at 60°C after final rinsing in acetone.
195
196 **2.3. Elemental analyses and Rock-Eval pyrolysis**
197
198 Bulk elemental analyses for carbon (± 0.4 wt.%) and hydrogen (± 0.2 wt.%)
199 contents were conducted by the SGS Company using thermal conductibility
200 according to ASTM D 5294.
201
202 Isolated OM was analyzed using Rock-Eval 6 (Vinci Technologies) following the
203 standard pyrolysis protocol described in Behar et al. (2001). Briefly, pyrolysis is
204 performed in a N_2 atmosphere and comprises two steps of pyrolysis, first an
205 isothermal phase held for 3 minutes followed by a rise in pyrolysis temperature
206 from 300 to 650 °C at a rate of 25°C.min^{-1}. After pyrolysis, the residual material
207 was then heated from 300 to 800 °C under purified air in an oxidation oven in
208 order to calculate TOC value (see Behar et al., 2001 for further details about
209 calculation procedure). During pyrolysis, the amounts of released effluents,
210 considered as hydrocarbons (HC) were continuously quantified by a flame
211 ionization detector [S1 and S2, for the first and second pyrolysis steps,
212 respectively, in mg HC/g of sample] while released CO and CO_2 were
213 continuously and simultaneously monitored by infrared detectors during both
214 pyrolysis (S3CO and S3CO_2) and combustion (S4CO and S4CO_2). The
215 quantification of the amounts of effluents led to the determination of the TOC

(wt.%) and of the Hydrogen Index (HI, defined as S2×100/TOC, in mg HC/g of TOC). The pyrolysis temperature associated with the maximum release of hydrocarbons, called "TpkS2" was determined. Note that we used TpkS2 rather than Tmax (Tmax= TpkS2– ΔTmax; Behar et al., 2001). For comparison, a ΔTmax of ca. 40 was used to turn Tmax values from the literature into TpkS2 values (Boussafir et al., 2012).

2.4. Raman microspectroscopy

The Raman study was performed using a Renishaw inVia micro-spectrometer equipped with a 532nm argon laser at 20 mW. The spectrometer was first calibrated using a silicon standard before each session. For each sample analysis, the laser was focused using a DMLM Leica microscope with a ×50 objective and the spectra were recorded in the 1000–1900 cm^{-1} Raman shift wavenumber range. The laser power at the sample surface was kept below 1 mW to prevent thermal alteration of kerogens (Everall et al., 1991).

2.5. NanoSIMS microprobe

The elemental composition of isolated OM was analyzed *in situ* using the CAMECA NanoSIMS 50 ion microprobe at the NanoSIMS facility of the Museum National d'Histoire Naturelle (MNHN) in Paris, France. For NanoSIMS measurements, isolated OM were pressed and coated with 20 nm of gold. Before each analysis, the sample surface was pre-sputtered using a 3 nA Cs^+ primary

beam current (ES3 = 30 μm; AS3 = 150 μm) in order to avoid surficial contamination and to achieve a saturation fluence of Cs^+, leading to constant secondary ion emissions (Thomen et al., 2014).

Analyses were then carried out using a *ca.* 300 pA Cs^+primary current on 40 μm × 40 μm areas (256 × 256 pixels), slightly smaller than the pre-sputtered areas in order to avoid pre-sputtering edge artifacts. Secondary $^{12}CH^-$, $^{12}C^{13}C^-$ and $^{12}C^{14}N^-$ were collected simultaneously in electron multipliers. A 15 % energy filtering was used to avoid overlapping between the $^{12}C^{13}C^-$ and $^{12}C^{12}CH^-$ secondary species peaks. All the NanoSIMS data were corrected for a 44 ns dead time on each electron multiplier and processed using the Limage software (developed by L. Nittler, Carnegie Institution, Washington DC, USA).

Areas where $^{12}CH^-$, $^{12}C^{13}C^-$ and $^{12}C^{14}N^-$ ionic species are co-emitted were selected in order to minimize any effect of residual hydrogenated minerals (that would only emit H but no C or N in the case of hydrated silicates, for example). In each analyzed area, 4 μm^2 regions of interest (ROIs) were defined.

Note that only five out of the eleven Archean kerogens were analysed by NanoSIMS due to facility availability. These five were selected either because (i) their bulk H/C atomic ratio values encompass values commonly reported for Archean kerogens or (ii) their anomalously high H/C atomic ratio values were assumed to result from the presence of hydrated minerals (Delarue et al., 2016).

2.6. Scanning Electron Microscopy

Isolated OM from the Panorama sample was resuspended in ethanol that was then pipetted and filtered on a polycarbonate filter (10 μm pore size). The polycarbonate filter was then directly gold coated (20 nm thick). Observations were performed with a TESCAN VEGA II SEM operating with an accelerating voltage of 15 kV at the Museum National d'Histoire Naturelle (MNHN) facility.

3. Results and Discussion

3.1. Hydrogen-to-Carbon ratios determined on isolated Archean organic matter

In the present set of studied isolated OM, H/C atomic ratios determined either by bulk analysis or using NanoSIMS range between 0.15 and 1.35 (Table 1). These values encompass H/C values usually reported on Archean kerogens (Hayes et al., 1983; Marshall et al., 2007; French et al., 2015; Ferralis et al., 2016). TOC values determined through Rock-Eval pyrolysis range between 3.7 and 51.0 wt.% (Table 1). Most of these values are close to those determined through elemental analyses (Delarue et al., 2016) except for GRW10 and GFWEX1-1b, for which Rock-Eval-derived TOC values are nearly half those previously determined using elemental analysis. This may be related to the heterogeneity of isolated OM in the test sample. In addition, the lowest TOC values (below 25%; Table 1) exhibited by some samples indicate that the acid treatment was not always efficient in removing the mineral matrix from the corresponding cherts. In these

cases, H/C ratio may be biased by some contribution of H originating from residual hydrogenated mineral(s), especially neoformed fluorides (Durand, 1980). By excluding mineral phases using molecular ions strictly related to OM, we obtain a linear relationship between $^{12}CH^-/^{12}C^{13}C^-$ ionic ratio and H/C ratio for the MGTKS3, 99SA07 and MGTKS1 samples (Fig. 1). This correlation suggests that the H/C ratio (ca. 1.35) of the 07SA22 isolated OM is largely overestimated (up to 800%) by residual hydrogenated minerals, as previously suspected (Delarue et al., 2016). In addition, the very low H/C ratio (0.15) computed by NanoSIMS is compatible with the very low HI determined by Rock-Eval pyrolysis, suggesting, in turn, that the HI value is not biased by these residual minerals.

Furthermore, based on this correlation, the measurement of the $^{12}CH^-/^{12}C^{13}C^-$ ionic ratio in the 4 of 03/08/85 isolated OM sample leads to a H/C ratio of ca. 0.64(Fig. 1). This value is consistent with the one previously determined by bulk elemental analysis on another sample from the Warrawoona Formation (PPRG006; H/C = 0.62; Derenne et al., 2008). Such a high H/C ratio has been suggested to be related to a significant contribution of aliphatic moieties linked to the kerogen matrix (Derenne et al., 2008). However, Marshall et al. (2007) questioned the origin of these compounds because the metamorphic grade undergone by the Warrawoona Formation (prehnite-pumpellyite to lower greenschist) may be too high to preserve such large amounts of aliphatics linked to the kerogen matrix. In the following, we used Rock-Eval pyrolysis to track the origin of hydrocarbons released upon pyrolysis of isolated Archean OM.

3.2. The "apparent" low thermal maturity of Isolated Archean organic matter: an influence of residual bitumen

For 7 out of the 10 studied Archean OM, HI-values are low, ranging between 2 and 22 mg HC/g of TOC (Table 1). Such values are in the same range as those reported by Brocks et al. (2003b) and they are in line with the low H/C ratio commonly observed in Archean kerogens. In contrast, the isolated OM from GRW10, MGTKS1 and 4 of 03/08/85 present rather high HI values of 65, 82 and 217 mg HC/g of TOC, respectively (Table 1). Moreover, these isolated Archean organic matter samples are the same as those which exhibit the highest H/C values (determined by elemental analysis and/or NanoSIMS), ranging from between 0.55 to 0.85 (Table 1).

The Zalesie Nowe kerogen is characterized by Rock-Eval parameters (HI=240 mg HC/g TOC and TpkS2 = 478 °C; Table 1) and an S2 Gaussian curve (Fig. 2) commonly observed for the thermal release of hydrocarbonaceous compounds covalently linked to the kerogen matrix of thermally-altered OM (Behar et al., 2001; Grundman et al., 2012). Note that this TpkS2 is close to those previously determined on this Silurian chert (TpKS2 = 482-488°C, i.e. Tmax = 442-448°C; Bauersachs et al., 2009). In contrast to this Silurian kerogen, the isolated Archean OM was characterized by pyrograms displaying shoulders and/or multimodal release of hydrocarbons (Fig. 2). Most of the isolated Archean OM exhibits a relatively high S1 peak followed by a less intense and large S2 peak with a maximum release of hydrocarbons ranging between ca. 326 and 448°C

(Fig. 2, Table 1). Such low TpkS2 values are at variance with the metamorphism up to greenschist metamorphism facies undergone by the host rocks. Indeed, the latter is associated with TpkS2 values higher than ca 475°C (Tmax = 436-464°C; Spangenberg and Frimmel, 2004). These pyrolytic features should then be regarded as anomalies.

Contamination by oil-based drilling mud lubricant is classically invoked to explain large S1 and S2 shoulders (Peters, 1986). However, this cause is unlikely to explain the high S1 peak and the release of hydrocarbons at low S2 pyrolysis temperature in the presently studied rocks as they were sampled from outcrop.

High S1 and especially S2 shoulders at low pyrolysis temperature may also be caused by the presence of indigenous thermolabile OM, such as residual heavy oil (Clementz, 1979) or solid bitumen (Sanei et al., 2015). In the following, the term "thermolabile" is used to account for the OM which is cracked at rather low temperature but which does not belong to the macromolecular network of the kerogen. Indeed, we cannot preclude the existence of non-volatile solid bitumen, the existence of which cannot be addressed by studying isolated OM. Indeed, further investigations studying OM in its mineralogical context are required (e.g. in situ approach; Bernard et al., 2012; Sanei et al., 2015). Although the aforementioned coexistence of solid bitumen is not excluded, S2 shoulders can be assigned to the presence of residual bitumen as evidenced by SEM in the Panorama sample. Indeed, the Panorama isolated OM is an ideal target when looking for non-thermally degraded bitumen because it underwent a mild-thermal alteration in comparison to other studied Archean OM, as revealed by comparison between Raman spectra (Delarue et al., 2016).

SEM imaging of the Panorama isolated OM reveals the existence of bitumen droplets as revealed by surface degassing features caused by the SEM beam (Fig. 3a). Despite the high fluorescence level rendering the Raman spectra less accurate (Fig. 3b), the bitumen droplets share a similar structural order with the surrounding OM (Fig. 3b), consistent with previous Raman spectra acquired on other OM samples from the Strelley Pool Formation (Lepot et al., 2013). In turn, we interpret these elements as showing that the bitumen underwent the same degree of thermal alteration as the host rock. It may thus be syngenetic, even though bitumen recovered in Archean rocks is commonly assigned to contamination. However, it also implies that residual bitumen and related hydrocarbons can bias the determination of the H content of the macromolecular structure of the Archean kerogens.

From a molecular point of view, and in contrast to previous studies stating that a first pyrolysis step at low temperature (ca. 300 to ca. 350°C) is enough to release thermolabile compounds (Brocks et al., 2003b; Marshall et al., 2007; Derenne et al., 2008), Rock-Eval pyrograms show that this first pyrolysis step is not systematically sufficient to ensure (i) the thermal desorption of the whole residual bitumen content, which can be trapped or adsorbed within/onto the surface of kerogen (Oehler et al. 1977), or (ii) the cracking of solid bitumen. Indeed, release of thermolabile OM still occurs at pyrolysis temperatures up to 400°C, when using the thermal degradation program of the Rock-Eval device. This echoes previous observations indicating that heavy fractions of petroleum release hydrocarbons in the 350 to 450°C range (Clementz, 1979). Considering that the study of the molecular composition of Archean hydrocarbons by

384 analytical pyrolysis was performed using a faster rise in pyrolysis temperature,
385 we suggest that the energy provided by pyrolysis at 300-350°C was not enough to
386 release the entire content of thermolabile hydrocarbons. Hence, the molecular
387 content observed at higher pyrolysis and in a faster rise in pyrolysis temperature
388 can encompass hydrocarbons originating from both (i) the pyrolysis of
389 thermolabile compounds and (ii) the thermal cleavage of the kerogen matrix.
390
391 **3.3. Evidence for multiple phases of OM by Rock-Eval pyrolysis**
392
393 In addition to the presence of S2 shoulders occurring at low pyrolysis
394 temperature, the pyrograms from the isolated Archean OM are characterized by
395 the release of hydrocarbon effluents at higher pyrolysis temperature, as reflected
396 by one or two well-defined S2 peaks ranging from between 471 and 586°C (Fig.
397 2). In total, 7 out of 10 isolated Archean OM samples are characterized by the
398 release of hydrocarbons in a narrow pyrolysis temperature range (576 to 586°C).
399 Such high pyrolysis temperatures are in line with the metamorphic grade
400 undergone by these Archean rocks, ranging between prehnite-pumpellyite to
401 greenschist facies (Marshall et al., 2007; Sugitani et al., 2007). They correspond
402 to the thermal cleavage of kerogen-bound hydrocarbon. Nonetheless, multiple
403 generation of hydrocarbons upon pyrolysis has also been observed in the GRW10,
404 MGTKS1up, MGTKS3 and the 4 of 03/08/85 isolated OM (Fig. 2). The multimodal
405 release of hydrocarbons points towards the existence of two distinct pools of OM
406 generating hydrocarbons at high pyrolysis temperature. This interpretation is
407 supported by the existence of two different types of OM within the GRW10 chert,

as revealed by both microscopy and *in situ* Raman spectroscopy (Figs. 3c,d) showing that OM dispersed within the mineral matrix and that from hydrothermal veins do not exhibit similar Raman first-order spectrum.

Indeed, in thermally-altered OM, the ratio between the intensities of the D and G bands (I_D/I_G) has been shown to describe the evolution of the structural order of OM during thermal alteration (Oberlin, 1984; Jehlicka and Bény, 1992; Jehlicka et al., 2003; Rouzaud et al., 2015). The Raman spectrum determined on OM contained within a mineral matrix is typically observed in OM that has undergone thermal alteration up to 320-350°C (Fig. 3d; Lahfid et al., 2010) and is, therefore, consistent with the greenschist facies metamorphism undergone by the metasediments from the Farrel Quartzite (Sugitani et al., 2007). In comparison to this OM, which exhibits an I_D/I_G ratio of ca. 1.5, OM from a hydrothermal vein presents a higher I_D/I_G ratio (ca. 2.0; Fig. 3d). Such a Raman spectrum is generally assigned to a metamorphic peak temperature above 400°C (Beyssac et al., 2002), suggesting that the "hydrothermal" OM has undergone a higher thermal alteration than OM from the mineral matrix. Note that in the following, we distinguish between primary hydrothermalism, i.e. contemporaneous hydrothermal activity (Westall et al., 2015a, 2015b), and secondary hydrothermalism occurring after rock formation. In addition to higher thermal alteration possibly related to secondary hydrothermalism, other factors may also imply changes in the structural order of OM. Studying OM from the 2.0 Gyr-old Zaonega Formation, Van Zuilen et al. (2012) showed that graphite films along mineral surfaces can even be formed under greenschist metamorphism facies usually associated with OM characterized by a lower structural order. For

these authors, peculiar geological conditions, such as hydrothermal circulation, can imply local changes in the structural order of OM. Although not fully understood, such local processes also likely explain the observed difference in the structural order between OM from the sedimentary matrix and from secondary hydrothermal veins.

Since OM from hydrothermal veins does not have the same structural order as OM from the sedimentary matrix, it is not possible to draw conclusions as to syngenecity of the two types. In turn, and in the absence of unequivocal criteria to determine its syngenecity, the occurrence of OM originating from hydrothermal veins must be taken into account to avoid any bias in the determination of the H/C atomic ratio of the kerogens related to OM from the main mineral matrix, especially in hydrothermally-altered metasediments such as Archean geological records. Therefore, characterization of the molecular content of Archean kerogens through thermal degradation should be performed on selected areas of the sample that are devoid of hydrothermal veins.

4. Conclusion

Rock-Eval pyrolysis of isolated OM from several Archean samples reveals the co-occurrence of various OM pools characterized by different thermal stabilities. In contrast to non-metamorphosed kerogen, as exemplified by the Zalesie Nowe kerogen, pyrolysis of the Archean OMs shows that they do not consist solely of hydrocarbons linked to the macromolecular structure of insoluble OM. Accordingly, the H/C atomic ratios determined on isolated Archean OM do not solely correspond to syngenetic hydrogenated organic compounds linked to the

kerogen matrix. Instead, they can also reflect the H composition of minerals as revealed by NanoSIMS, of thermally labile residual bitumen and/or solid bitumen, and of OM from secondary hydrothermal veins generating hydrocarbons at high pyrolysis temperature, for which syngenecity is still an open issue. Because of the low amount of hydrocarbons linked to the syngenetic Archean kerogen matrix, any residual trace of bitumen or OM from secondary hydrothermal veins can bias the use of the H/C ratio associated with the macromolecular network. This study shows that Rock-Eval pyrolysis provides a useful tool (i) to evaluate the significance of H/C atomic ratio as a proxy for hydrocarbon preservation in Archean kerogens, and also (ii) to better constrain the source of hydrocarbons released during thermal analytical degradation providing in turn, a frame for future molecular investigations.

Acknowledgements

This research is supported by the ERC Grant No. 290861 – PaleoNanoLife (P.I. F. Robert; ERC Grant No. 290861). The National NanoSIMS Facility at the MNHN is supported by MNHN, CNRS, Région Ile de France, and Ministère de l'Enseignement Supérieur et de la Recherche. Authors are grateful to Sylvain Pont for SEM imaging. The authors express their gratitude to V. Rouchon and O. Belhadj (Center for Research on the Preservation of Collections, USR 3224) for Raman spectroscopy. We also thank C.P. Marshall, J.A. Curiale and an anonymous reviewer for their insightful comments.

Figure captions

Figure 1: Linear relationship between the $^{12}CH^-/^{12}C^{13}C^-$ ionic ratio determined with NanoSIMS and bulk H/C atomic ratio determined with bulk analyses. Using the linear relationship between the $^{12}CH^-/^{12}C^{13}C^-$ molecular ionic ratio and bulk H/C atomic ratio, the H/C atomic ratio values of sample 07SA22 (ca 0.15) and of sample 4 of 03/08/85 (ca 0.64) kerogen samples were computed. Error bars represent the standard errors related to the mean $^{12}CH^-/^{12}C^{13}C^-$ ionic ratio determined on selected regions of interest (ROI).

Figure 2: Rock Eval pyrograms of Silurian (0.42 Gyr-old) and Archean (3.0 to 3.5 Gyr-old) silicified cherts. Left column shows the whole pyrograms and the corresponding TpkS2 values (bold character). Right column focuses on the hydrocarbon released/generated during the second step of pyrolysis involving a rise in pyrolysis temperatures from 300 to 650 °C at a rate of 25°C.min^{-1}. TpkS2 values are indicated in bold character whereas other pyrolysis temperatures associated with a release of hydrocarbons are indicated in regular character.

Figure 3: (a) SEM image of a bitumen droplet recovered within the Panorama kerogen. (b) Raman spectra measured on the bitumen droplet presented in Fig 3a and on surrounding OM. (c) GRW10 thin section photography illustrating the existence of hydrothermal veins cutting siliclastic successive deposits (mineral matrix). (d) Raman spectra determined on OM from the mineral matrix (red Raman spectra) and from the hydrothermal vein (blue Raman spectra) observed within the GRW10 thin section presented in (c)

References

Bauersachs, T., Kremer, B., Schouten, S., Damste, J.S.S., 2009. A biomarker and $\delta^{15}N$ study of thermally altered Silurian cyanobacterial mats. Organic Geochemistry 40, 149-157.

Behar, F., Beaumont, V., Penteado, H.L.D., 2001. Rock-Eval 6 technology: Performances and developments. Oil & Gas Science and Technology-Revue D Ifp Energies Nouvelles 56, 111-134.

Bernard, S., Wirth, R., Schreiber, A., Schulz, H.M., Horsfield, B., 2012. Formation of nanoporous pyrobitumen residues during maturation of the Barnett Shale (Fort Worth Basin). International Journal of Coal Geology 103, 3-11.

Beyssac, O., Goffe, B., Chopin, C., Rouzaud, J.N., 2002. Raman spectra of carbonaceous material in metasediments: a new geothermometer. Journal of Metamorphic Geology 20, 859-871.

Bourbin, M., Derenne, S., Gourier, D., Rouzaud, J.N., Gautret, P., Westall, F., 2012. Electron Paramagnetic Resonance Study of a Photosynthetic Microbial Mat and Comparison with Archean Cherts. Origins of Life and Evolution of Biospheres 42, 569-585.

Bourbin, M., Derenne, S., Robert, F., 2012a. Limits in pyrolysis-GC-MS analysis of kerogen isolated from Archean cherts. Organic Geochemistry 52, 32-34.

Bourbin M., 2012. Carbonaceous Matter in Archean Siliceous Sedimentary Rocks: from the Origins of Life on Earth to Exobiological Perspectives. Ph. D. thesis, University Paris Diderot.

,M., Sifeddine, A., Jacob, J., Foudi, M., Cordeiro, R.C., Albuquerque, A.L.S., Abrao, J.J., Turcq, B., 2012. Petrographical and geochemical study of modern lacustrine sedimentary organic matter (Lagoa do Caco, Maranao, Brazil): Relationship between early diagenesis, organic sedimentation and lacustrine filling. Organic Geochemistry 47, 88-98.

Brocks, J.J., Logan, G.A., Buick, R., Summons, R.E., 1999. Archean molecular fossils and the early rise of eukaryotes. Science 285, 1033-1036.

Brocks, J.J., Love, G.D., Snape, C.E., Logan, G.A., Summons, R.E., Buick, R., 2003b. Release of bound aromatic hydrocarbons from late Archean and Mesoproterozoic kerogens via hydropyrolysis. Geochimica Et Cosmochimica Acta 67, 1521-1530.

Brocks, J.J., Buick, R., Logan, G.A., Summons, R.E., 2003a. Composition and syngeneity of molecular fossils from the 2.78 to 2.45 billion-year-old Mount Bruce Supergroup, Pilbara Craton, Western Australia. Geochimica Et Cosmochimica Acta 67, 4289-4319.

Clementz, D.M., 1979. Effect of oil and bitumen saturation on source-rock pyrolysis. Aapg Bulletin-American Association of Petroleum Geologists 63, 2227-2232.

Curiale, J.A., 1986. Origin of solid bitumens, with emphasis on biological marker results. Organic Geochemistry 10, 559–580.

Delarue, F., Robert, F., Sugitani, K., Tartese, R., Duhamel, R., Derenne, S., 2017. Investigation of the Geochemical Preservation of ca. 3.0 Ga Permineralized and Encapsulated Microfossils by Nanoscale Secondary Ion Mass Spectrometry. Astrobiology 17, 1192-1202.

551 Delarue, F., Rouzaud, J.N., Derenne, S., Bourbin, M., Westall, F., Kremer, B.,
552 Sugitani, K., Deldicque, D., Robert, F., 2016. The Raman-Derived Carbonization
553 Continuum: A Tool to Select the Best Preserved Molecular Structures in Archean
554 Kerogens. Astrobiology 16, 407-417.
555 Delvaux, D., Martin, H., Leplat, P., Paulet, J., 1990. Comparative Rock-Eval
556 pyrolysis as an improved tool for sedimentary organic matter analysis. Organic
557 Geochemistry 16, 1221–1229.
558 Derenne, S., Robert, F., Skrzypczak-Bonduelle, A., Gourier, D., Binet, L.,
559 Rouzaud, J.-N., 2008. Molecular evidence for life in the 3.5 billion year old
560 Warrawoona chert. Earth and Planetary Science Letters 272, 476-480.
561 Durand, B. (Ed.), 1980. Kerogen, Insoluble Organic Matter from Sedimentary
562 Rocks. Editions Technip 27, Paris, p. 519.
563 Espitalie, J., Deroo, G., Marquis, F., 1985a. Rock-Eval pyrolysis and its
564 application .2. Revue de l'Institut Francais Du Petrole 40, 755-784.
565 Espitalie, J., Deroo, G., Marquis, F., 1985b. Rock-Eval pyrolysis and its
566 application. Revue de l'Institut Francais Du Petrole 40, 563-579.
567 Espitalie, J., Deroo, G., Marquis, F., 1986. Rock-Eval pyrolysis and its application
568 .3. Revue de l'Institut Francais Du Petrole 41, 73-89.
569 Espitalie, J., Laporte, J.L., Madec, M., Marquis, F., Leplat, P., Paulet, J.,
570 Boutefeu, A., 1977. Rapid method for source rocks characterization and for
571 determination of petroleum potential and degree of evolution. Revue de l'Institut
572 Francais Du Petrole 32, 23-42.

573 Everall, N.J., Lumsdon, J., Christopher, D.J., 1991. The effect of laser-induced
574 heating upon the vibrational raman-spectra of graphites and carbon-fibers.
575 Carbon 29, 133-137.
576 Ferralis, N., Matys, E.D., Knoll, A.H., Hallmann, C., Summons, R.E., 2016.
577 Rapid, direct and non-destructive assessment of fossil organic matter via
578 microRaman spectroscopy. Carbon 108, 440-449.
579 French, K.L., Hallmann, C., Hope, J.M., Schoon, P.L., Zumberge, J.A., Hoshino,
580 Y., Peters, C.A., George, S.C., Love, G.D., Brocks, J.J., Buick, R., Summons, R.E.,
581 2015. Reappraisal of hydrocarbon biomarkers in Archean rocks. Proceedings of
582 the National Academy of Sciences of the United States of America 112, 5915-
583 5920.
584 Grundman, G., Behar, F., Malo, M., Baudin, F., Lorant, F., 2012. Evaluation of
585 hydrocarbon potential of the Paleozoic (Cambrian-Devonian) source rocks of the
586 Gaspe Peninsula, Quebec, Canada: Geochemical characterization, expulsion
587 efficiency, and erosion scenario. AAPG Bulletin 96, 729-751.
588 Hackley, P.C., Cardott, B.J., 2016. Application of organic petrography in North
589 American shale petroleum systems: a review. International Journal of Coal
590 Geology 163, 8–51.
591 Han,Y., Mahlstedt, N.,Horsfield, B., 2015. The Barnett Shale: Compositional
592 fractionation associated with intraformational petroleum migration, retention,
593 and expulsion. AAPG Bulletin 99, 2173–2202.
594 Hayes, J. M., Kaplan, I. R. and Wedeking, K. W. (1983) Precambrian organic
595 geochemistry, preservation of the record. In: Schopf J.W. (Ed.), Earth's Earliest
596 Biosphere, Princeton University Press, Princeton, pp. 93–134.

Jacob, H., 1989. Classification, structure, genesis and practical importance of natural solid oil bitumen ("migrabitumen"). International Journal of Coal Geology 11, 65–79.

Jarvie, D.M. (2012) Shale resource systems for oil and gas : part 2-shale-oil resource systems. In: Breyer, J.A. (Ed.), Shale Reservoirs- Giant Resources for the 21st Century, AAPG Memoir 97, pp 89-119.

Jehlicka, J., Beny, C., 1992. Application of raman microspectrometry in the study of structural-changes in precambrian kerogens during regional metamorphism. Organic Geochemistry 18, 211-213.

Jehlicka, J., Urban, O., Pokorny, J., 2003. Raman spectroscopy of carbon and solid bitumens in sedimentary and metamorphic rocks. Spectrochimica Acta Part a-Molecular and Biomolecular Spectroscopy 59, 2341-2352.

Kremer, B., Kazmierczak, J., 2005. Cyanobacterial mats from silurian black radiolarian cherts: Phototrophic life at the edge of darkness? Journal of Sedimentary Research 75, 897-906.

Lahfid, A., Beyssac, O., Deville, E., Negro, F., Chopin, C., Goffe, B., 2010. Evolution of the Raman spectrum of carbonaceous material in low-grade metasediments of the Glarus Alps (Switzerland). Terra Nova 22, 354-360.

Ledevin, M., Arndt, N., Simionovici, A., Jaillard, E., Ulrich, M., 2014. Silica precipitation triggered by clastic sedimentation in the Archean: new petrographic evidence from cherts of the Kromberg type section, South Africa. Precambrian Research 255, 316–334.

Lepot, K., Williford, K.H., Ushikubo, T., Sugitani, K., Mimura, K., Spicuzza, M.J., Valley, J.W., 2013. Texture-specific isotopic compositions in 3.4 Gyr old organic

matter support selective preservation in cell-like structures. Geochimica Et Cosmochimica Acta 112, 66-86.

Marshall, C.P., Love, G.D., Snape, C.E., Hill, A.C., Allwood, A.C., Walter, M.R., Van Kranendonk, M.J., Bowden, S.A., Sylva, S.P., Summons, R.E., 2007. Structural characterization of kerogen in 3.4 Ga Archaean cherts from the Pilbara Craton, Western Australia. Precambrian Research 155, 1-23.

Oberlin, A., 1984. Carbonization and graphitization. Carbon 22, 521-541.

Oehler, J.H., 1977b. Irreversible contamination of precambrian kerogen by c-14-labeled organic-compounds. Precambrian Research 4, 221-227.

Peters, K.E., 1986. Guidelines for evaluating petroleum source rock using programmed pyrolysis. Aapg Bulletin-American Association of Petroleum Geologists 70, 318-329.

Rasmussen, B., Fletcher, I.R., Brocks, J.J., Kilburn, M.R., 2008. Reassessing the first appearance of eukaryotes and cyanobacteria. Nature 455, 1101-U1109.

Romero-Sarmiento, M.-F., Pillot, D., Letort, G., Lamoureux-Var, V., Beaumont, V., Huc, A.-Y., Garcia, B., 2015. New Rock-Eval method for characterization of unconventional shale resource systems. Oil & Gas Science and Technology. http://dx.doi.org/10.2516/ogst/2015007

.Rouzaud, J.N., Deldicque, D., Charon, E., Pageot, J., 2015. Carbons at the heart of questions on energy and environment: A nanostructural approach. Comptes Rendus Geoscience 347, 124-133.

Sanei, H., Wood, J.M., Ardakani, O.H., Clarkson, C.R., Jiang, C.Q., 2015. Characterization of organic matter fractions in an unconventional tight gas siltstone reservoir. International Journal of Coal Geology 150, 296-305.

Spangenberg, J.E., Frimmel, H.E., 2001. Basin-internal derivation of hydrocarbons in the Witwatersrand Basin, South Africa: evidence from bulk and molecular delta C-13 data. Chemical Geology 173, 339-355.

Sugitani, K., Grey, K., Allwood, A., Nagaoka, T., Mimura, K., Minami, M., Marshall, C.P., Van Kranendonk, M.J., Walter, M.R., 2007. Diverse microstructures from Archaean chert from the mount goldsworthy-mount grant area, pilbara craton, western australia: Microfossils, dubiofossils, or pseudofossils? Precambrian Research 158, 228-262.

Sugitani, K., Mimura, K., Takeuchi, M., Lepot, K., Ito, S., Javaux, E.J., 2015. Early evolution of large micro-organisms with cytological complexity revealed by microanalyses of 3.4Ga organic-walled microfossils. Geobiology 13, 507-521.

Tartese, R., Chaussidon, M., Gurenko, A., Delarue, F., Robert, F., 2017. Warm Archean oceans reconstructed from oxygen isotope composition of early-life remnants. Geochemical Perspectives Letters 3, 55-65.

Thomen, A., Robert, F., Remusat, L., 2014. Determination of the nitrogen abundance in organic materials by NanoSIMS quantitative imaging. Journal of Analytical Atomic Spectrometry 29, 512-519.

van Zuilen, M.A., Fliegel, D., Wirth, R., Lepland, A., Qu, Y.G., Schreiber, A., Romashkin, A.E., Philippot, P., 2012. Mineral-templated growth of natural graphite films. Geochimica Et Cosmochimica Acta 83, 252-262.

Ventura, G.T., Kenig, F., Reddy, C.M., Schieber, J., Frysinger, G.S., Nelson, R.K., Dinel, E., Gaines, R.B., Schaeffer, P., 2007. Molecular evidence of Late Archean archaea and the presence of a subsurface hydrothermal biosphere. Proceedings of

668 the National Academy of Sciences of the United States of America 104, 14260-
669 14265
670 Westall, F., de Ronde, C.E.J., Southam, G., Grassineau, N., Colas, M., Cockell,
671 C.S., Lammer, H., 2006. Implications of a 3.472-3.333 Gyr-old subaerial microbial
672 mat from the Barberton greenstone belt, South Africa for the UV environmental
673 conditions on the early Earth. Philosophical Transactions of the Royal Society B-
674 Biological Sciences 361, 1857-1875.
675 Westall, F., Campbell, K.A., Breheret, J.G., Foucher, F., Gautret, P., Hubert, A.,
676 Sorieul, S., Grassineau, N., Guido, D.M., 2015a. Archean (3.33 Ga) microbe-
677 sediment systems were diverse and flourished in a hydrothermal context.
678 Geology 43, 615-618.
679 Westall, F., Foucher, F., Bost, N., Bertrand, M., Loizeau, D., Vago, J.L., Kminek,
680 G., Gaboyer, F., Campbell, K.A., Breheret, J.G., Gautret, P., Cockell, C.S., 2015b.
681 Biosignatures on Mars: What, Where, and How? Implications for the Search for
682 Martian Life. Astrobiology 15, 998-1029.
683

Table 1: Rock-Eval-derived parameters (S1, S2, TpkS2, TOC and HI) and H/C atomic ratios determined on Silurian (0.42 Gyr-old) and Archean (3.0 to 3.5 Gyr-old) silicified cherts. H/C ratios were determined with bulk elemental analysis and with NanoSIMS using the ratio between the $^{12}C^{13}C^-$ and $^{12}C_2^-$ molecular ionic species. "n.d." indicates that parameter was not determined.

Sample name	Geological Formation, country	Age (Gyr)	S1 (mg/g)	S2 (mg/g)	TpkS2 (°C)	TOC (w.%)	HI (mg/g TOC)	H/C (Bulk analysis)	$^{12}C^{13}C^-/^{12}C_2^-$	H/C (NanoSIMS)
ZALESIE	Zalesie Nowe, Poland	0.42	2.6	122.5	478	51.1	240	0.95	n.d.	n.d.
GGR2	Farrel Quartzite, Australia	3.0	0.5	0.9	386	18.5	5	0.42	n.d.	n.d.
GRW10	Farrel Quartzite, Australia	3.0	12.0	19.1	326	29.5	65	0.55	n.d.	n.d.
ORW9	Farrel Quartzite, Australia	3.0	0.5	1.1	433	20.7	5	0.38	n.d.	n.d.
GFWEX1-1b	Farrel Quartzite, Australia	3.0	1.0	3.0	368	17.1	18	0.31	n.d.	n.d.
MGTKS1up	Farrel Quartzite, Australia	3.0	2.4	5.5	586	40.8	14	0.30	n.d.	n.d.
MGTKS1	Farrel Quartzite, Australia	3.0	36.1	30.8	372	37.7	82	0.85	7.4	0.85
MGTKS3	Farrel Quartzite, Australia	3.0	0.4	0.9	582	46.9	2	0.24	1.8	0.23
99SA07	Kromberg, South Africa	3.3	n.d.	n.d.	n.d.	n.d.	n.d.	0.39	3.4	0.40
07SA22	Hoeggonoeg, South Africa	3.4	0.3	0.7	395	17.6	4	1.35	1.1	0.15
Panorama	Strelley Pool, Australia	3.4	4.6	5.4	448	24.2	22	n.d.	n.d.	n.d.
4 of 03/08/85	Warrawoona, Australia	3.5	2.3	8.0	471	3.7	217	n.d.	5.5	0.64

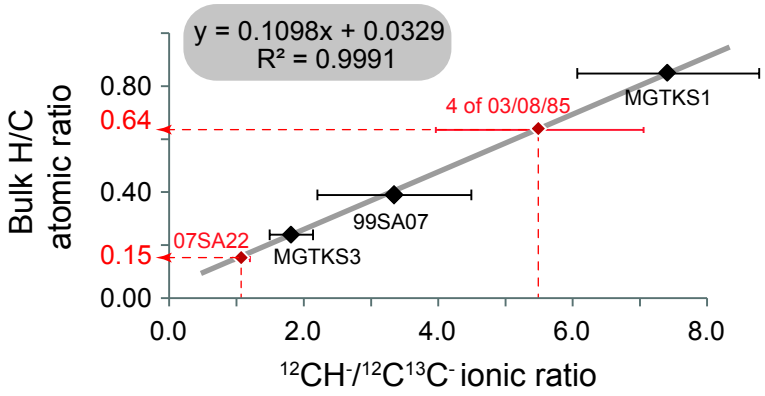
y = 0.1098x + 0.0329
R² = 0.9991
Bulk H/C
atomic ratio
0.80
0.64
0.40
0.15
0.00
0.0
2.0
4.0
6.0
8.0
4 of 03/08/85
MGTKS1
99SA07
07SA22
MGTKS3
12CH-/12C13C- ionic ratio

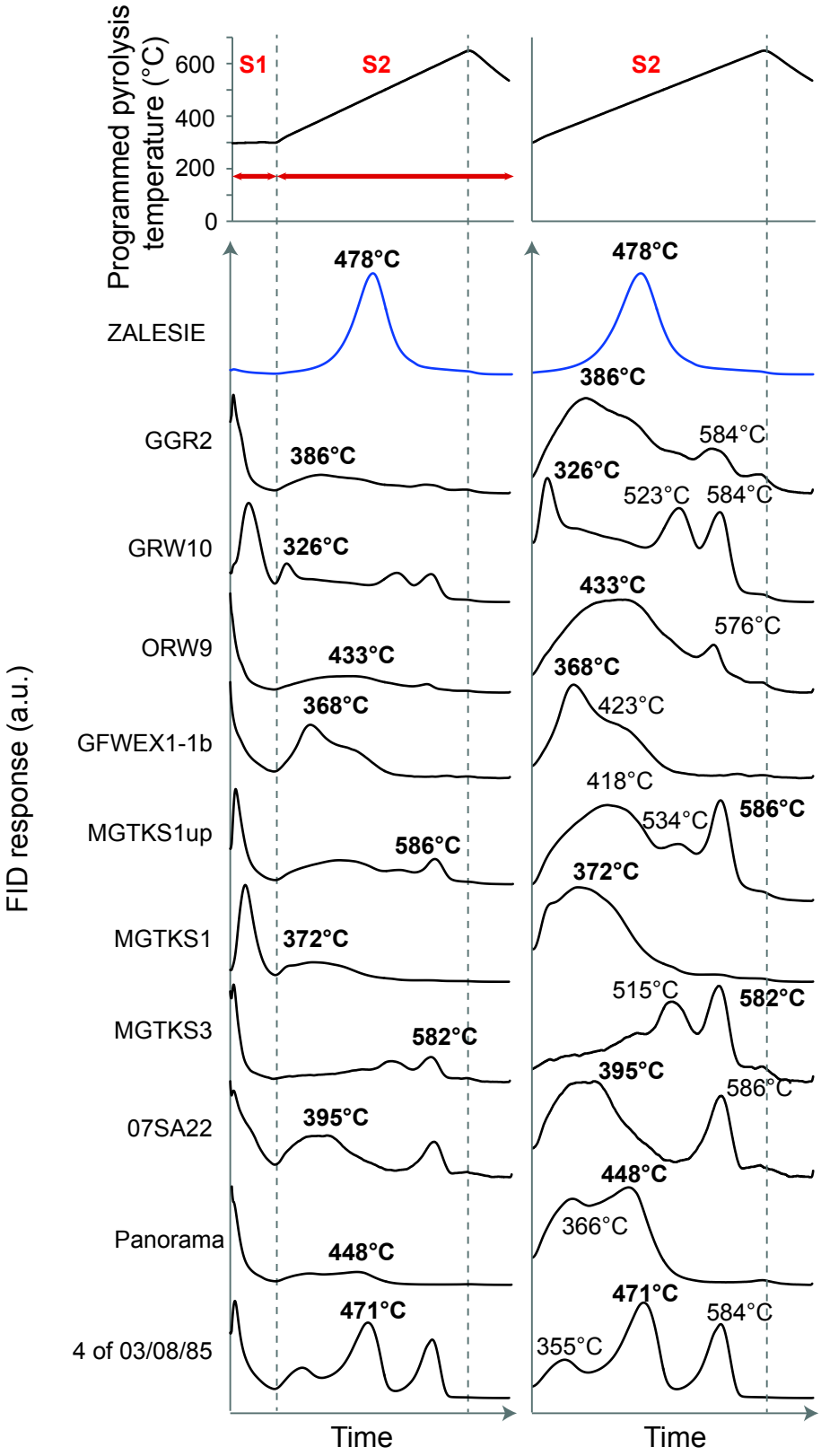
Programmed pyrolysis temperature (°C)
600
400
200
0
S1
S2
S2
FID response (a.u.)
ZALESIE
478°C
478°C
GGR2
386°C
386°C
584°C
GRW10
326°C
326°C
523°C
584°C
ORW9
433°C
433°C
576°C
GFWEX1-1b
368°C
368°C
423°C
MGTKS1up
586°C
418°C
534°C
586°C
MGTKS1
372°C
372°C
MGTKS3
582°C
515°C
582°C
07SA22
395°C
395°C
586°C
Panorama
448°C
448°C
366°C
4 of 03/08/85
471°C
471°C
584°C
355°C
Time
Time

a.

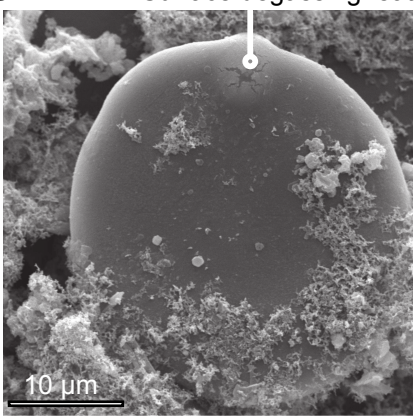
Surface degassing feature
10 µm

b.

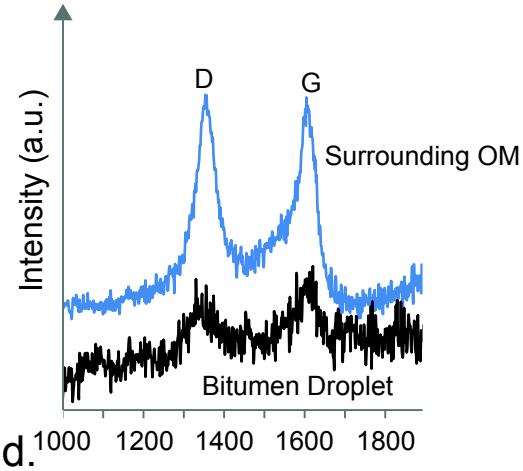
D
G
Surrounding OM
Intensity (a.u.)
Bitumen Droplet
1000
1200
1400
1600
1800

c.

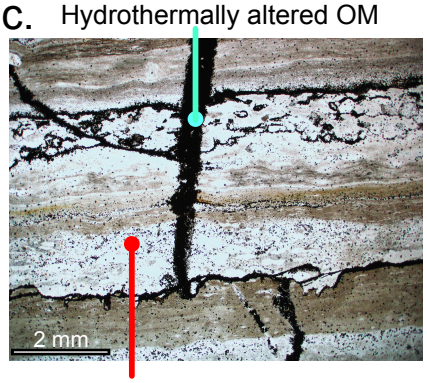
Hydrothermally altered OM
2 mm
Sedimentary OM

d.

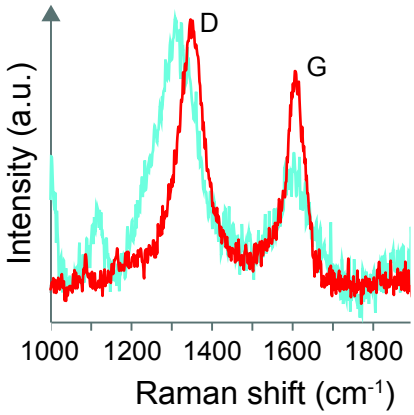
D
G
Intensity (a.u.)
1000
1200
1400
1600
1800
Raman shift (cm-1)